International Journal of advancement in electronics and computer engineering (IJAECE)
Volume 4, Issue 12, April, 2016, pp.712-717, ISSN 2278 -1412

A Novel Image Fusion Technique Using Multi Resolution Analysis (MRI) Neural Networks

Kalpana Rai[1], Dr. S. Bhuvaneshvari[2]

[1] *Research Scholar, Department of Computer science and Engineering, Pondicherry University, India;*

[2] *Professor, Department of Computer science and Engineering, Pondicherry University, India;*

***Abstract*—Present work describes a promising method in image fusion remote sensing applications. Due to intrinsic properties of neural networks (DNN) in image reconstruction, a novel Image Fusion Technique presents based on multi resolution analysis (MRA) framework. First, a low resolution Panchromatic (LR Pan) image is constructed using its high resolution (HR) version. Then, the relationship between LR/HR Pan images are used to reconstruct the HR Multispectral (MS) image utilizing the LR MS. For our work, two datasets are considered and for each of them, the effect of several parameters such as window size, overlapping percentage and number of training samples on spectral distortion are considered. After training DNN, the LR MS image is given to the trained network as input to obtain MS image with better spatial details and finally the fused image obtains using MRA framework. Comparison with state of art methods, the proposed method has better results from objective and visual perspectives.**

Keywords—Pansharpening; multi resolution analysis; neural networks

I. INTRODUCTION

Remote sensing is a field of study whose goals are related to measure the changes of the earth for different applications such as image fusion [1-2], land cover segmentation [3-4]. There are many satellites which provide images for mentioned applications. One of the main interests of many researchers and hot topics, is pansharpening [5]. Due to bandwidth limitation, the satellites cannot provide an image with both high spatial and spectral resolutions, but they can simultaneously collect two types of images with two different sensors; one of them has high spatial resolution which is called Pan image and the other one has high spectral resolution under name MS image. Pansharpening aims to fuse LR MS image with HR Pan image to obtain an image which inherits both information [6]. Image fusion is also used in medical applications [7-8].

Image Fusion Techniques basically can be classified into two main groups [9]: Components substitution (CS) methods and multi resolution analysis (MRA) methods. In both CS and MRA approaches, a detail map should be extracted and then should be injected to the resampled MS image. These methods have similar frameworks except in the extraction of detail maps. In CS method, the detail map is obtained by the difference between the Pan image and the linear combination of resampled MS bands. On the other hand, in MRA methods the detail map is computed using the difference between Pan image and its low resolution version through decomposition of Pan image using wavelet transforms, Laplacian pyramids and some other techniques. The main problem in the pansharpening approaches is the reduction of spatial distortions while preserving spectral information. The CS methods such as intensity-hue-saturation (IHS) [10], principle component analysis (PCA) [11], and Gram-Schmidt (GS) [12], have good spatial information but suffer from spectral distortions. Apart from CS methods, MRA methods such as indusion [13], 'à trous' wavelet transform (ATWT) [14] and Laplacian pyramid (LP) [15], have good spectral details while suffer from spatial distortions.

In the present work, deep neural networks (DNN) are employed to find the relationship between original Pan image patches and its resampled version. After training the DNN, the resampled MS image patches are given to the network as input. In our proposed scheme, the effect of several parameters such as window size, overlapping percentage and number of training samples in the output of trained network is considered for analyzing spectral distortion. It is shown that for different datasets, these parameters can be different. So, the best results for each one are reported. It should be mentioned that training of DNN have a huge computational cost. We perform our proposed method using graphics processing unit (GPU) for speed up the run time. The DNN has two step learning [16]: pretraining and fine-tuning. The pretraining stage can be done using restricted Boltzmann machines (RBM) [17] and sparse denoising autoencoders (SDA) [18]. In the fine-tuning stage, the whole network trains again using backpropagation algorithm in a supervised manner to find optimal weights of the network [19].

The rest of the paper is organized as follows: Section II describes the basic mathematical modeling and tools for the proposed method, consisting proposed scheme and basic concepts of DNN. Effect of several parameters such as window size, overlapping percentage and number of training samples on spectral distortion for two datasets are provided in Section III. In section IV the fusion process of the proposed method is compared with state of art methods objectively and visually.

Finally, conclusion is provided in section V.

II. MATHEMATICAL MODELING AND TOOLS

A. Proposed Pansharpening Framework

Basic framework of MRA approaches as described in many previous works is as follows [10]:

$$MS_k^H = MS_k^L + g_k(P - P^{LR}) \quad (1)$$

where MS_k^H is the fused product corresponds to k^{th} band, MS_k^L is the k^{th} band of resampled MS image, g_k is the adjusting gain of the k^{th} detail map, P is the original Pan image and P^{LR} is a low resolution version of Pan image. In the recent years, there has been proposed several works on computing P^{LR} and g_k to obtain better fusion results.

In this paper, P^{LR} is computed using the resampled version of Pan image. First, the Pan image is downsampled by factor N and then upsampled with inverse of N. By utilizing the relationship between P^{LR} and Pan image, a neural network is trained. It is assumed that relationship between the P^{LR} and Pan image is the similar to the relationship between resampled MS image and its high resolution version. From this assumption, the high resolution version of resampled MS image can be directly computed using trained network, which is called SMS_k. So, we modify the equation (1) as follows:

$$MS_k^H = SMS_k + g_k(P - P^{LR}) \quad (2)$$

The final product of the proposed method can be achieved using Eq. 2.

B. Sparse Coding and Denoising Autoencoders

An autoencoder is a type of neural networks with backpropagation algorithm for unsupervised learning. Thegoal of using autoencoder is trying to reconstruct the input. Fig. 1 shows an autoencoder. As shown in Fig. 1, an autoencoder takes an input $x \in [0,1]$ and first maps it (with an encoder) to a hidden representation $y \in [0,1]$ as the following equation

$$y = s(Wx + b) \quad (3)$$

where $s(x)$ is sigmoid activation function. The coded data (y), is then mapped back (with a decoder) into a reconstruction zof the same shape as x using the following equation

$$z = s(W'y + b') \quad (4)$$

with this optionally assumption that $W = W'$. The hidden representation tries to extract basic features of the input data. The denoising autoencoder is a stochastic type of the autoencoder. In fact, a denoising autoencoder has two main tasks: try to encode the input (the input are coded stochastically using certain distribution), and try to undo the effect of a corruption process stochastically applied to the input of the autoencoder.

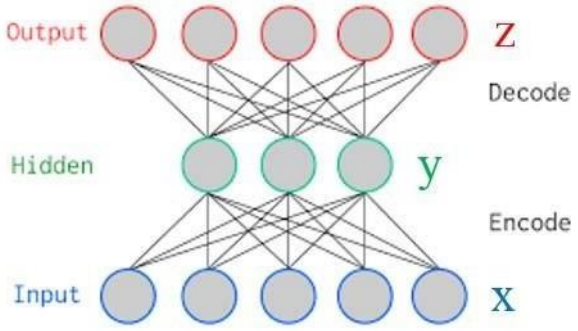

Fig. 1. A simple scheme of an autoencoder.

The latter can only be done by capturing the statistical dependencies between the inputs [20].

Combining sparse coding and denoising autoencoder first proposed by Xie *et al.* [18] for image denoising and blind inpainting. The idea behind the sparse denoising is to better feature extraction using these constraints.

In this paper, main features of the low resolution Pan are extracted and try to reconstruct it using neural networks. $\{x_p^i\}_{i=1}^N$ and $\{z_p^i\}_{i=1}^N$ are considered as the patches of LR and reconstructed LR Pan image respectively. To obtain the $T = \{W, W', b, b'\}$, neural networks trained using the following objective function

$$F_1\left(\{x_p^i, z_p^i\}_{i=1}^N; T\right) = \frac{1}{N}\sum_{i=1}^{N}\left\|z_p^i - \hat{z}(x_p^i)\right\|^2 + \frac{\lambda}{2}\left\|W\right\|^2 + \beta\sum_{\rho}\mathrm{KL}(\rho\,\|\,\hat{\rho}) \quad (5)$$

where λ and β are adjusting parameters, the second term is weight decaying term, and the third term $\mathrm{KL}(\rho \,\|\, \hat{\rho})$ is the sparsity term, which is defined as

$$\mathrm{KL}(\rho\,\|\,\hat{\rho}) = \rho\log\frac{\rho}{\hat{\rho}} + (1-\rho)\log\frac{1-\rho}{1-\hat{\rho}} \quad (6)$$

and $\hat{\rho} = \frac{1}{N}\sum_{i=1}^{N} s(x_p^i)$ is the average activation of hidden layer.

After training the first autoencoder, the second autoencoder can be trained using the features which are extracted from the first autoencoder as the input.

After training each autoencoder, they can be stacked to each other as a series of autoencoders and trained again with the initial weights obtained from the previous pre-training. The whole network is then trained again for global fine-tuning to minimize the following function

$$F_2\left(\{u_p^i, z_p^i\}_{i=1}^N; T\right) = \frac{1}{N}\sum_{i=1}^{N}\left\|u_p^i - \hat{z}(x_p^i)\right\|^2 + \frac{\lambda}{2}\sum_{j=1}^{M}\left\|W_j\right\|^2 \quad (7)$$

where $\{u_{p\,i=1}^{i\,N}$ is HR Pan image patches, M is number of stacked sparse denoising autoencoder and W_j show the weights corresponds to j^{th} layer in the neural networks.

In both pre-training and fine-tuning stages, scaled conjugate gradient (SCG) is used for optimizing the objective functions (5) and (7).

III. Experiment on several parameters for QuickBird and WorldView-3 datasets

In this section, the effect of several parameters such as window size, overlapping percentage and number of training samples is investigated for QuickBird and WorldView-3 datasets as shown in Fig. 2. For QuickBird dataset, Pan and MS images have 0.7-m and 2.8-m resolutions respectively. For WorldView-3 satellite, Pan and MS images have 0.31-m and 1.24-m resolutions respectively. For conducting our experiment, the size of Pan image for both datasets is 1024×1024 pixels and the corresponding MS images have 256×256 pixels. Wald's protocol is followed in our proposed fusion process. For all experiments, we use the mean squares error (MSE) as a metric for describing the spectral distortion. The MSE of test image and its result are averaged over 5 times computation and are reported in the followingtables.

A. Effect of Window Size on Datasets

The effect of window size on the value of averaged MSE are analyzed in this part. For our experiment we consider the

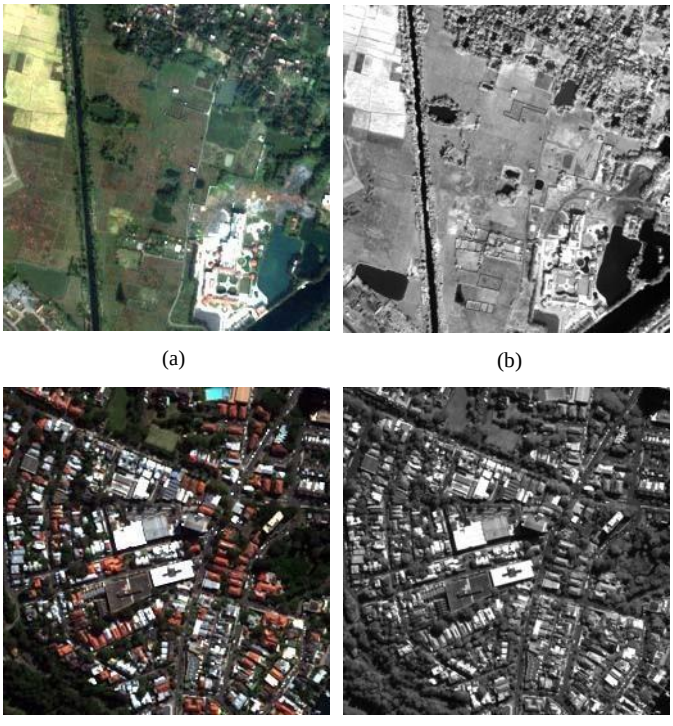

(a) (b)

(c) (d)

Fig. 2. Datasets. (a) Original MS image (QuickBird), (b) Original Pan image (QuickBird) (c) Original MS image (WorldView-3) (d) Original Pan image (WorldView-3).

TABLE I
Effect of window size on the spectral distortion

Window size	No. of training samples	MSE (Training)	MSE (1st band)	MSE (2nd band)	MSE (3rd band)
3×3	32768	0.0101	0.2823	0.3113	0.2573
3×3	49152	0.0101	0.2847	0.3121	0.2596
5×5	14450	0.0103	0.2241	0.1906	0.2190
5×5	21675	0.0098	**0.1902**	**0.1739**	**0.1853**
7×7	8192	0.0095	0.2177	0.2052	0.1953
7×7	12288	0.0094	0.2304	0.1989	0.2022
9×9	5202	0.0097	0.2181	0.2183	0.1986
9×9	7803	**0.0093**	0.2286	0.1948	0.1607

TABLE II
Effect of overlapping percentage on the spectral distortion

Window size	Overlapping	MSE (Training)	MSE (1st band)	MSE (2nd band)	MSE (3rd band)
3×3	1 (40%)	0.0101	0.2823	0.3113	0.2573
3×3	2 (50%)	0.0099	0.2649	0.2937	0.2277
5×5	2 (40%)	0.0103	0.2241	0.1906	0.2190
5×5	3 (50%)	0.0103	0.2341	0.2563	0.1978
5×5	4 (70%)	0.0099	0.3815	0.3522	0.3216
7×7	3 (40%)	0.0095	0.2177	0.2052	0.1953
7×7	4 (50%)	0.0097	0.2238	0.2159	0.2196
7×7	5 (70%)	0.0097	**0.1513**	**0.1522**	**0.1205**
9×9	4 (40%)	0.0097	0.2181	0.2183	0.1986
9×9	5 (50%)	**0.0093**	0.2793	0.2337	0.2133
9×9	6 (70%)	0.0094	0.1990	0.1800	0.1818

TABLE III
Effect of training samples on the spectral distortion

Window size	No. of Samples	MSE (Training)	MSE (1st band)	MSE (2nd band)	MSE (3rd band)
3×3	16384	0.0101	0.2796	0.3071	0.2531
3×3	32768	0.0101	0.2823	0.3113	0.2573
3×3	49152	0.0101	0.2847	0.3121	0.2596
3×3	65536	0.0101	0.2832	0.3104	0.2574
3×3	81920	0.0101	0.2858	0.3148	0.2611
5×5	7225	0.0105	0.2789	0.2999	0.2485
5×5	14450	0.0103	0.2241	0.1906	0.2190
5×5	21675	0.0098	0.1902	0.1739	0.1853
5×5	28900	0.0096	**0.1890**	**0.1671**	0.1772
5×5	36125	0.0103	0.3206	0.3512	0.3035
7×7	4096	0.0095	0.2211	0.2042	0.2023
7×7	8192	0.0095	0.2177	0.2052	0.1953
7×7	12288	0.0094	0.2304	0.1989	0.2022
7×7	16384	**0.0092**	0.2184	0.1972	**0.1572**
7×7	20480	**0.0092**	0.2451	0.2161	0.2217
9×9	2601	0.0095	0.1975	0.1775	0.1625
9×9	5202	0.0097	0.2181	0.2183	0.1986
9×9	7803	0.0093	0.2286	0.1948	0.1607
9×9	10404	0.0096	0.2077	0.1951	0.1781
9×9	13005	**0.0092**	0.2507	0.2092	0.1884

window sizes 3, 5, 7 and 9. In this stage, each sample patch is trained twice randomly. So, for all the window sizes the number of training samples are fixed and equals to 2, 3 times of the generating patches. Another notable thing is the overlapping percentage. The value of overlapping percentage is

also fixed and equals to 40% for each window size. Table I & IV show the results of the changing window size. As clear, the window size 5×5 and 7×7 has the less spectral distortions than the others for QuickBird and WorldView-3 respectively. The window size has a direct relationship with the sizes and the amount of details in the image. For crowded image, like urban and land-cover areas the smaller window sizes have better results. The best value of the MSE is reported in bold form.

B. Effect of Overlapping Percentage on Datasets

In this sub-section, the effect of overlapping percentage on the datasets is evaluated. For this purpose, three different overlapping percentages of 40%, 50% and 70% are considered. The number of training samples is equal to 2 times of generating patches for each window size. Table II & V show the results of mentioned experiment for QuickBird and WorldView-3 respectively. As reported, by increasing the value of overlapping percentage, spectral distortions become less. There is another key point which should be mentioned. Larger value of overlapping percentage may cause overfitting such what is happened in the window size 5×5 with 70% overlapping in Table II.

C. Effect of Training Samples on Datasets

At the final experiment on datasets, the effect of number of training samples in the value of MSEs is investigated. Overlapping percentage is set to 40%. Table III & VII show the results of changing training samples. For example, in WorldView-3 results as in Table VI the window size 5×5 with 3 times of generating patches has less spectral distortion. The effect of training samples show that the spectral distortion become less until overfitting occurs. We consider the best parameters for the fusion process.

IV. FUSION RESULTS

In this section, the results of previous section are employed in the fusion process. The chosen initial settings for the QuickBird and WorldView-3 datasets are reported in Table VII and Table VIII respectively. The proposed method compares with state of art methods like GS [12], PCA [11], IHS [10], and indusion [13] objectively and visually. There are several spectral and spatial metrics to objectively assess the fused products. In this paper, correlation coefficient (CC) [21], error relative global adimensionnelle de synthese (ERGAS) [22], spectral angle mapper (SAM) [23], relative average spectral error (RASE) [24], structural similarity (SSIM) [25] and universal image quality index (UIQI) [26] are used for comparison. The results of pansharpening process for QuickBird datasets are reported in Fig. 3 and the corresponding objective quality assessment for the implemented methods are provided in Table IX. For visual assessment comparison, the proposed method can better preserve the reference image colors such as the white regions in the right corner. The spatial details of the Pan image are also better injected to the proposed pansharpened image. From objective point of view, the quality metrics of the proposed method can have better results relatively in comparison with state of art methods. For the WorldView-3 dataset, the results of fusion results are provided in Fig. 4 and the objective assessment of the pansharpened images are reported in Table X. For the WorldView-3 dataset, the colors of the ceilings and grass regions in the proposed method are more similar to reference image than the other methods. The edges and spatial details of the Pan image are better added to the proposed method. The comparison of quality metrics for WorldView-3 dataset shows that the proposed method has better results than other methods.

TABLE IV

Effect of window size on the spectral distortion

Window size	No. of training samples	MSE (Training)	MSE (1st band)	MSE (2nd band)	MSE (3rd band)
3×3	32768	0.0135	0.4627	0.3911	0.4056
3×3	49152	0.0135	0.4659	0.3940	0.4092
5×5	14450	0.0135	0.4625	0.3944	0.3831
5×5	21675	0.0137	**0.4273**	**0.3561**	**0.3436**
7×7	8192	**0.0129**	0.5627	0.4752	0.4643
7×7	12288	0.0130	0.5437	0.4565	0.4433
9×9	5202	0.0148	0.5516	0.4721	0.4607
9×9	7803	0.0131	0.6019	0.5116	0.5021

TABLE V

Effect of overlapping percentage on the spectral distortion

Window size	Overlapping	MSE (Training)	MSE (1st band)	MSE (2nd band)	MSE (3rd band)
3×3	1 (40%)	0.0135	0.4627	**0.3911**	0.4056
3×3	2 (50%)	0.0136	0.5470	0.4715	0.4911
5×5	2 (40%)	0.0135	**0.4625**	0.3944	**0.3831**
5×5	3 (50%)	0.0135	0.5169	0.4379	0.4257
5×5	4 (70%)	0.0135	0.4899	0.4133	0.3989
7×7	3 (40%)	0.0129	0.5627	0.4752	0.4643
7×7	4 (50%)	0.0135	0.5117	0.4314	0.4218
7×7	5 (70%)	0.0137	0.5623	0.4782	0.4670
9×9	4 (40%)	0.0148	0.5516	0.4721	0.4607
9×9	5 (50%)	0.0139	0.6439	0.5472	0.5440
9×9	6 (70%)	0.0133	0.5323	0.4508	0.4414

TABLE VI

Effect of training samples on the spectral distortion

Window size	No. of Samples	MSE (Training)	MSE (1st band)	MSE (2nd band)	MSE (3rd band)
3×3	16384	0.0135	0.4670	0.3944	0.4099
3×3	32768	0.0135	0.4627	0.3911	0.4056
3×3	49152	0.0135	0.4659	0.3940	0.4092
3×3	65536	0.0135	0.4535	0.3824	0.3926
3×3	81920	0.0135	0.4814	0.4086	0.4258
5×5	7225	0.0135	0.5073	0.4287	0.4369
5×5	14450	0.0135	0.4625	0.3944	0.3831
5×5	21675	0.0137	**0.4273**	**0.3561**	**0.3436**
5×5	28900	0.0137	0.4449	0.3700	0.3578
5×5	36125	0.0136	0.4537	0.3847	0.3796
7×7	4096	0.0130	0.5781	0.4861	0.4692
7×7	8192	**0.0129**	0.5627	0.4752	0.4643
7×7	12288	0.0130	0.5437	0.4565	0.4433
7×7	16384	0.0129	0.6167	0.5175	0.4994
7×7	20480	0.0130	0.5279	0.4592	0.4487
9×9	2601	0.0133	0.5694	0.4848	0.4726
9×9	5202	0.0148	0.5516	0.4721	0.4607
9×9	7803	0.0131	0.6019	0.5116	0.5021
9×9	10404	0.0132	0.5817	0.4967	0.4849
9×9	13005	0.0136	0.5387	0.4553	0.4487

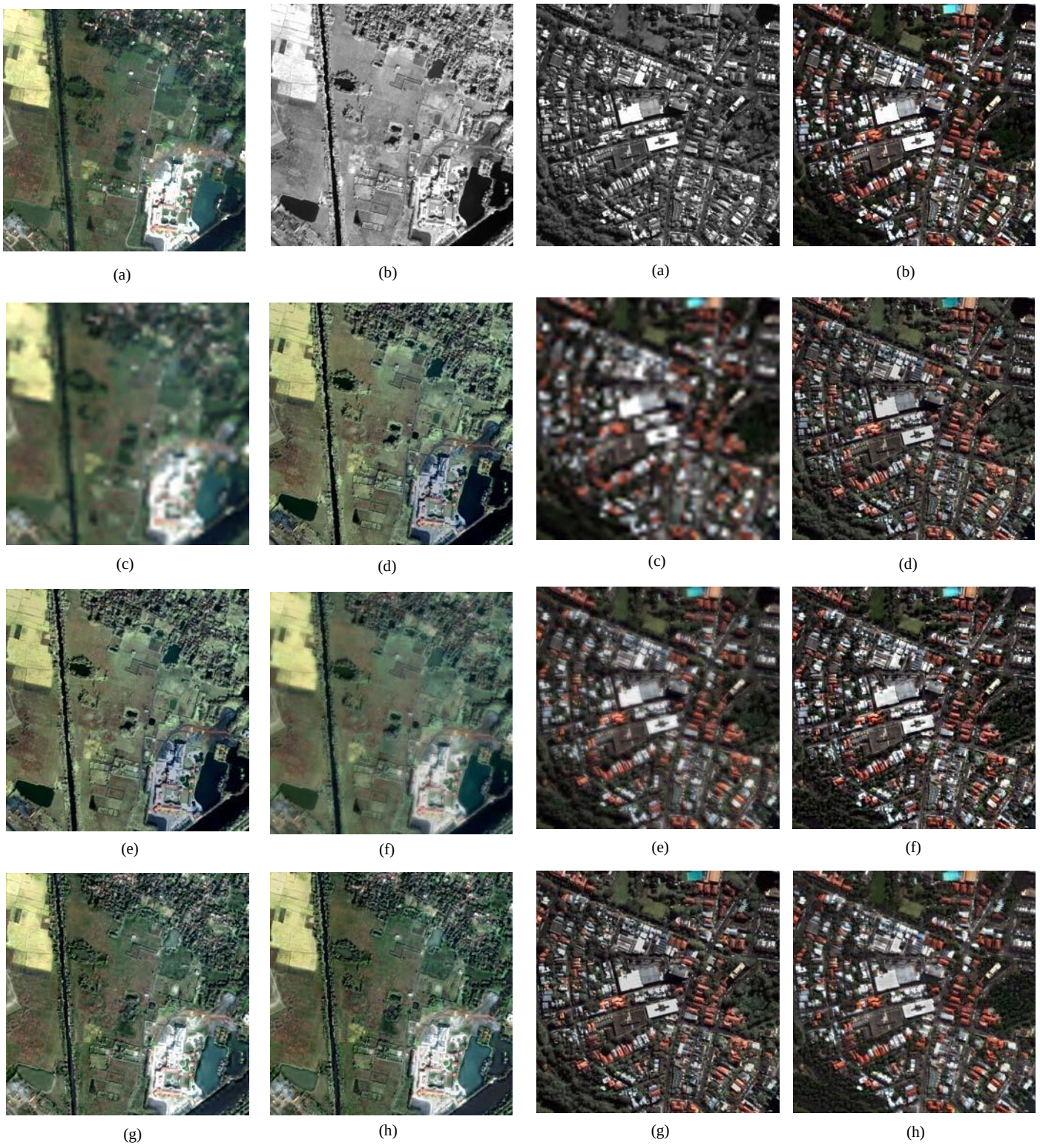

(a) (b) (c) (d) (e) (f) (g) (h)

Fig. 3. Fusion results for QuickBird Dataset. (a) Original MS image (b) Original Pan image (c) Resampled MS image (d) GS method (e) PCA method (f) IHS method (g) Indusion method (h) Proposed method.

(a) (b) (c) (d) (e) (f) (g) (h)

Fig. 4. Fusion results for WorldView-3 Dataset. (a) Original MS image (b) Original Pan image (c) Resampled MS image (d) GS method (e) PCA method (f) IHS method (g) Indusion method (h) Proposed method.

TABLE VII
Initial settings for the QuickBird dataset

Window size	7×7
Overlapping percentage	70%
Number of training samples	31752

TABLE VIII
Initial settings for the WorldView-3 dataset

Window size	5×5
Overlapping percentage	40%
Number of training samples	21765

TABLE IX
Fusion results for the QuickBird satellite

	CC	RASE	ERGAS	SAM	SSIM	UIQI
GS	0.606	47.535	11.933	11.652	0.416	0.615
PCA	0.610	47.239	11.857	11.477	0.417	0.618
IHS	0.862	27.929	7.053	**5.194**	**0.596**	0.853
Indusion	0.854	29.983	7.554	7.526	0.513	0.858
DNN	**0.885**	**26.408**	**7.043**	6.542	0.579	**0.888**

TABLE X
Fusion results for the WorldView-3 satellite

	CC	RASE	ERGAS	SAM	SSIM	UIQI
GS	0.927	37.173	9.377	6.427	0.775	0.897
PCA	0.927	37.180	9.378	6.429	0.775	0.897
IHS	0.940	36.965	9.280	**5.515**	0.748	0.893
Indusion	0.943	30.490	7.710	10.840	0.787	0.940
DNN	**0.961**	**27.996**	**6.720**	6.168	**0.815**	**0.946**

V. CONCLUSION

In this paper, a novel Image Fusion Technique is proposed using multi resolution analysis framework and neural networks. After obtaining the relationship between Pan image and its low resolution version using DNN, the high resolution version of resampled image can directly compute by trained network. In our future work, we focus on optimizing the injected detail maps for better pansharpening.

REFERENCES

[1] H. Ghassemian, "A retina based multi-resolution image-fusion." *Geoscience and Remote Sensing Symposium, 2001. IGARSS'01. IEEE 2001 International*. Vol. 2. IEEE, 2001.

[2] H. Ghassemian, "Multi-sensor image fusion using multirate filter banks." *Image Processing, 2001. Proceedings. 2001 International Conference on*. Vol. 1. IEEE, 2001.

[3] F. Mirzapour, and H. Ghassemian. "Object-based multispectral image segmentation and classification." *Telecommunications (IST), 2014 7th International Symposium on*. IEEE, 2014.

[4] S. Niu, et al. "Robust noise region-based active contour model via local similarity factor for image segmentation." *Pattern Recognition*, vol. 61, pp. 104-119, Jan. 2017.

[5] H. Ghassemian. "A review of remote sensing image fusion methods." *Information Fusion*, vol. 32, pp. 75-89, Nov. 2016.

[6] M. Ghahremani, and H. Ghassemian. "A Compressed-Sensing-Based Pan-Sharpening Method for Spectral Distortion Reduction." *IEEE Transactions on Geoscience and Remote Sensing*, vol. 54, no. 4, pp. 2194-2206, Nov. 2015.

[7] S. Daneshvar, , and H. Ghassemian. "MRI and PET images fusion based on human retina model." *Journal of Zhejiang University-SCIENCE A*, vol. 8, no. 10, pp. 1624-1632, 2007.

[8] S. Daneshvar, , and H. Ghassemian. "Fusion of MRI and PET images using retina based multi-resolution transforms." *Signal Processing and Its Applications, 2007. ISSPA 2007. 9th International Symposium on*. IEEE, 2007.

[9] G. Vivone, et al. "A critical comparison among pansharpening algorithms." *IEEE Transactions on Geosci. and Remote Sens.*, vol. 53, no. 5, pp. 2565-2586, May 2015.

[10] W. Carper, T. Lillesand, and R. Kiefer, "The use of intensity-huesaturation transformations for merging SPOT panchromatic and multispectral image data," *Photogramm. Eng. Remote Sens.*, vol. 56, no. 4, pp. 459–467, Apr. 1990.

[11] Jr. P. S. Chavez, and A. W. Kwarteng, "Extracting spectral contrast in Landsat thematic mapper image data using selective principal component analysis," *Photogramm. Eng. Remote Sens.*, vol. 55, no. 3, pp. 339–348, Mar. 1989.

[12] C. A. Laben and B. V. Brower, "Process for enhancing the spatial resolution of multispectral imagery using pan-sharpening," U.S. Patent6 011 875, 2000.

[13] M. M. Khan, , J. Chanussot, , L. Condat, and A. Montavert, , "Indusion: Fusion of multispectral and panchromatic images using the induction scaling technique," *IEEE Geosci. Remote Sens. Lett.*, vol. 5, no. 1, pp. 98–102, Jan. 2008.

[14] M. J. Shensa, , "The discrete wavelet transform: Wedding the à trous and Mallat algorithm," *IEEE Trans. Signal Process.*, vol. 40, no. 10, pp. 2464–2482, Oct. 1992.

[15] P. J. Burt, and E. H. Adelson, , "The Laplacian pyramid as a compact image code," *IEEE Trans. Commun.*, vol. 31, no. 4, pp. 532–540, Apr. 1983.

[16] B. A. Olshausen, and D. J. Field. "Sparse Coding with an Overcomplete Basis Set: A Strategy Employed by V1." *Vision Research*, Vol. 37, pp. 3311–3325, Dec. 1997.

[17] R. Salakhutdinov, , A. Mnih, , and G. Hinton,. "Restricted Boltzmann machines for collaborative filtering." *Proceedings of the 24th international conference on Machine learning*. ACM, 2007.

[18] J. Xie, , L. Xu, and E. Chen. "Image denoising and inpainting with deep neural networks." *Advances in Neural Information Processing Systems*. 2012.

[19] M. F. Moller, "A Scaled Conjugate Gradient Algorithm for Fast Supervised Learning", *Neural Networks*, vol. 6, 1993, pp. 525–533.

[20] Pascal Vincent, et al. "Extracting and composing robust features with denoising autoencoders." *Proceedings of the 25th international conference on Machine learning*. ACM, 2008.

[21] H. R. Shahdoosti, and H. Ghassemian. "Combining the spectral PCA and spatial PCA fusion methods by an optimal filter." *Information Fusion*, vol. 27 , pp. 150-160, Jan. 2016.

[22] L. Alparone, S. Baronti, A. Garzelli, and F. Nencini, "A global quality measurement of pan-sharpened multispectral imagery," *IEEE Geosci. Remote Sens. Lett.*, vol. 1, no. 4, pp. 313–317, Oct. 2004.

[23] R. H. Yuhas, A. F. H. Goetz, and J. W. Boardman, "Discrimination among semi-arid landscape endmembers using the Spectral Angle Mapper (SAM) algorithm," *in Proc. Summaries 3rd Annu. JPL Airborne Geosci. Workshop*, pp. 147–149, 1992.

[24] H. R. Shahdoosti, and H. Ghassemian. "Fusion of MS and PAN images preserving spectral quality." *IEEE Geoscience and Remote Sensing Letters*, vol. 12, no. 3, pp. 611-615, Mar. 2015.

[25] Z. Wang, et al. "Image quality assessment: from error visibility to structural similarity." *IEEE Transactions on Image Processing*, vol. 13, no. 4, pp. 600-612, Apr. 2004.

[26] Z. Wang and A. C. Bovik, "A universal image quality index," *IEEE Signal Process. Lett.*, vol. 9, no. 3, pp. 81–84, Mar. 2002.